ISSN 1392 - 1207. MECHANIKA. 2013 Volume 19(2): 215-222

Proposed method to acquire an extended diagram for a gasoline engine

I. Mihai, I.C. Manolache-Rusu
Stefan cel Mare University, Universitatii 13, 720229 Suceava, Romania, E-mail: mihai.i@fim.usv.ro

crossref http://dx.doi.org/10.5755/j01.mech.19.2.4151

1. Obtaining the pressure signal by experiment

One of the methods to analyze the internal combustion processes involves visualizing the pressure evolution inside the cylinder depending on the rotation angle of the crankshaft. The object of present research is finding a method to obtain an extended diagram without machining the engine cylinder heads. In order to draw diagram $p - \alpha$ also known as extended diagram, we designed and built a piezoelectric transducer that allows measuring the pressure at values below 4500 kPa. For this step we measured the sensing element of the transducer using thin membrane stability computations. In Fig. 1 we present a cross-section of the pressure transducer and we also point out its components alongside with its real image.

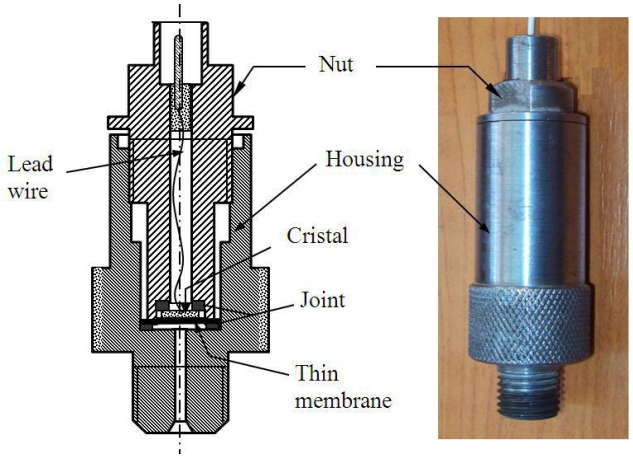

Fig. 1 Pressure transducer

Based on the piezoelectric effect we can ascertain that within the transducer electric charges develop on the crystal surface when pressure acts on it. The polarization that develops in these conditions shall be proportional to the amount of applied force. Moreover, a polarity shift occurs depending on how the applied force is oriented. The distortion that occurs within the crystal lattice causes the previously mentioned piezoelectric effect and also produces damage to the electric balance that exists between the atoms that form the lattice.

In the build stage we used piezoelectric elements [1-3] represented by disks made out of barium titanate. They were pre-strained between the membrane and the sensing element body. The pressure will push towards the thin membrane, will deform the membrane and will generate a force that pushes against the piezoelectric disks. At all times an electric charge that is proportional to the pressure within the engine cylinder shall be generated.

2. Description of the experimental test bench

To conduct an experimental study, a test bench was designed (shown in Fig. 2).

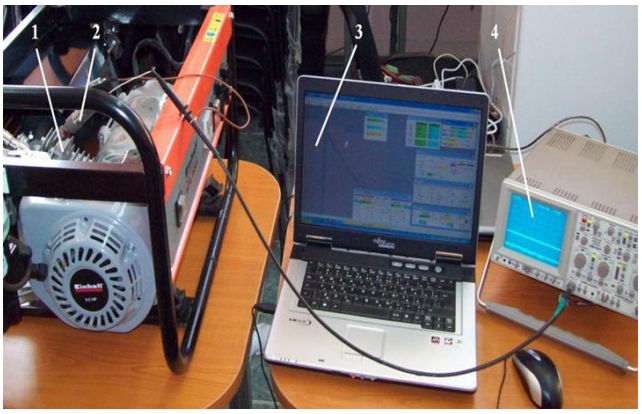

Fig. 2 Overview of the experimental test bench

The most important elements of the experimental test bench are: STE2000 a four-stroke single cylinder engine – *1*, pressure transducer – *2*, a laptop – *3* and an HAMEG 1507-2 oscilloscope with memory and interface RS232 – *4*. Since the pressure transducer must be connected directly to the pressure within the cylinder we searched for a noninvasive solution. In this respect we adopted the idea which involved modifying the engine spark plug in such a way that it enabled us to connect through it to the transducer. Such a method has several advantages. The most important advantage is that the cylinder heads no longer need to be dismounted from the engine. In addition, it is no longer necessary to drill and thread holes in the cylinder head in order to mount the transducer, which could modify mechanical structures and temperature fields. It must also be mentioned that the modifications brought to the spark plug can be successfully done in any laboratory with minimal equipment. It was found experimentally that the adopted method doesn't have an effect on the generation of electrical sparks and the engine works under normal conditions, without interruptions or any other noticeable deficiencies. No pressure oscillation phenomena were found along the conduit linking the modified spark plug to the piezoelectric transducer. Supplementary, this conduit can be subjected to a water cooling process in order to avoid transducer overheating. Engine vibrations didn't influence the proper functioning of the pressure transducer. To achieve this we went through several stages. A regular spark plug was first dismantled, and then modified as illustrated in Fig. 3. The modifications consist of machining a small channel in the ceramic part of the spark plug, corresponding to the threaded hole in which the transducer will be mounted.

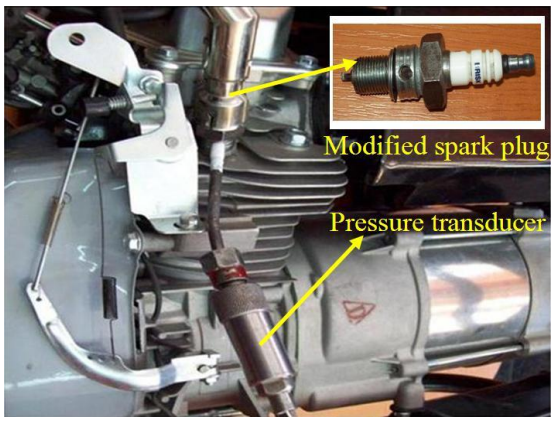

Fig. 3 Modified spark plug installed on the engine and pressure transducer

Mounting spark and the pressure transducer on the test ring are shown in Fig. 3. In the same figure we also show the generator that can be powered in order to act as electric brake. In order to adjust the speed it is required to have the possibility to fine tune the load connected to the generator in order to cover the entire scale of revolutions provided by the heat engine.

3. Experimental methodology, conditions, equipment and its calibration

In the case of internal combustion engines, the pressure variation speed inside a cylinder during the beginning of the combustion process (ignition) can reach values of 50000÷150000 daN/cm^2 s which imposes the use of equipment with high pass frequencies in order to accurately describe the periodically variable physical parameter. The frequency domain can be determined starting from a harmonic analysis of the physical parameter in order to define the rank of the last significant harmonic from a series development. If *s* denotes the rank of this harmonic, and *f*, Hz represents the frequency of cycles, the highest frequency of the necessary passing bandwidth can be determined as:

$$f_s = sf \ . \tag{1}$$

As the variation slope of the measured parameter by report to time increases, the number of terms in a series development, *s*, must be higher. If a four stroke engine ($\tau = 4$) is considered working at a speed of n = 5500 rot/min, its frequency is given by:

$$f = \frac{2n}{\tau 60} . \tag{2}$$

By taking into consideration that approximately 100 harmonics are necessary to correctly describe the pressure diagram, the frequency of the first harmonic is determined as follows:

$$f_s = s\frac{n}{2\times 60} = 4.583 \text{ kHz} . \tag{3}$$

In order to ensure an adequate bandwidth for passing frequencies, according to Table 1, the characteristic frequency of the installation must be much higher.

Table 1

Influence of frequency ratio f_n/f_s on the relative attenuation of *s* ranked harmonic, $\Delta A_s/A_s$

f_n / f_s	10	7.15	4.6	3.3	2.1	1.8
$\Delta A_s/A_s$	1	2	5	10	30	50

If the frequency of the first harmonic was determined to be of 4.583 kHz, than according to Table 1, it can be assessed that the installation characteristic frequency is 45.83 kHz.

Piezoelectric pressure transducers must be calibrated in order to determine the linear dependency between applied pressure and the electrical signal yielded at transducer output, measured as the shift of the spot of an oscilloscope. To that end, a hydraulic calibration device was employed. The calibration was conducted in similar running conditions, and using the same cable to link the transducer to the oscilloscope and with the oscilloscope knobs and switches in the same positions. The hydraulic calibration device consists of an oil tank from which the pressure chamber is fueled. The pressure applied to the transducer is measured using a standardized pressure gauge. Pressure is applied in predetermined increments over the full range of the pressure transducer. The pressure transducer voltage output is compared at each increment to a pressure gauge reading. The experimental evaluation of pressures applied to the transducer and to the standardized gauge was done with respect to the rules imposed by the Procedure for calibrating pressure transducers USBR 1050-89. During the experimental investigations, room temperature inside the laboratory varied with less than ±10°C, the equipments were brought inside the laboratory 24 hours before the experiments and were plugged in 30 min in advance before staring measurements. The following steps were followed:

1. The measurement data were filled in a form.
2. The pressure range to be calibrated was determined and recorded.
3. The transducer was connected to the same pressure source as the standardized pressure gauge.
4. A transducer signal reading was made and recorded without applying any pressure.
5. The increment was determined by report to the measuring range using Table 2.
6. For each increment, pressure was applied to the system and readings were recorded for applied pressure and readout response.
7. Measurements were repeated for pressures decreasing towards zero.
8. The pressure transducer error and percent error for each pressure increment were calculated and evaluated.

Fig. 4 illustrates results obtained during calibration.

Table 2

Recommended pressure increments for calibrated pressure transducers - USBR 1050-89

Pressure range		Pressure increment	
lbf/in^2	kPa	lbf/in^2	kPa
0 - 200	0 - 1400	25	175
200 -1000	1400 - 7000	100	700

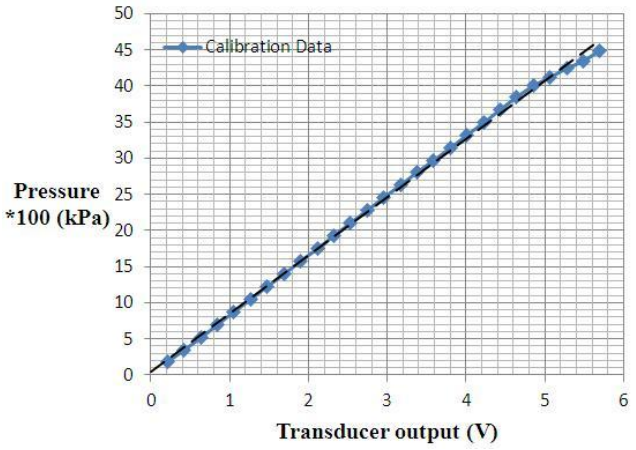

Fig. 4 Calibration of the 0–4485 kPa piezoelectric pressure transducer

It was found that the transducer outputs at 175 kPa a minimum voltage of 0.211 V while the maximum output, at 4485 kPa was of 5.7 V. If δp is the pressure differential across the ports and the output is linear [4], the pressure at any intermediate voltage can be computed from:

$$\frac{\delta p - \delta p_{min}}{\delta p_{max} - \delta p_{min}} = \frac{V_{out} - V_{min}}{V_{max} - V_{min}} \tag{4}$$

The measured pressure difference [4], can be determined as follows:

$$\delta p = \delta p_{min} + \frac{\delta p_{max} - \delta p_{min}}{4}\left(V_{out} - 1\right). \tag{5}$$

Eq. (5) allows to accurately transforming the output voltage of the transducer to pressures.

The residual for data point *i* is:

$$r_i = \delta p_{fit,i} - \delta p_i \,. \tag{6}$$

The manufacturer [4] claims that the maximum transducer error is less than 0.25%. The total uncertainty in the pressure value obtained with the transducer is:

$$u_{tot} = \sqrt{u_{cal}^2 + u_{fit}^2} \,. \tag{7}$$

In Eq. (7), the calibration error is determined by:

$$u_{cal} = \left(\delta p_{min} - \delta p_{max}\right) max\left(f_{ses}\right), \tag{8}$$

where f_{ses} represents the full scale error specification. The u_{fit} term in Eq. (6) represents the error in using our conversion equation to predict the calibration data and can be determined using the following expression:

$$u_{fit} = max\left|\delta p_i - \left[\delta p_{min} + \frac{\delta p_{max} - \delta p_{min}}{4}\left(V_i - 1\right)\right]\right| \tag{9}$$

Knowing that $r_{max} = max|r_i|$, results obtained using the error assessment methodology are illustrated in Table 3.

Table 3
Values of maximum residual, maximum error, calibration error and total uncertainty

Transducer	r_{max}	$r_{s,\,max}$	u_{cal}	u_{tot}
Piezoelectric	7.18×10^{-4}	7.47×10^{-4}	1.27×10^{-3}	1.53×10^{-3}

As the total error was found to be less than 1%, this shows that the used transducer fits in the precision class of laboratory equipment.

4. Dynamic phenomena analysis in the gas column of the pressure transducer connecting channel

The presence of the transducer connecting channel can represent a source for errors in the recording of cylinder pressures [5]. The gas column under pressure or depression circulates in a dynamic regime from the cylinder towards the transducer membrane. This way, a pressure difference appears between the pressure from the measuring point, p_i and the one applied to the membrane p_m. This pressure drop occurs due to frictions along the gas route, due to the non stationary flow regime which leads to oscillations and to a pressure gradient along the gas column.

Due to the presence of a gas column, a delay τ occurs in the transducer response by report to real moment of signal generation. If the channel length is considered l and the speed of sound w_a , then $\tau = l/w_a$. If the gas state parameters are considered then $w_a = (kp/\rho)^{1/2}$. For the analysis of the dynamic effects it is considered that no significant variations of pressures p_i and p_m occur in time and that the volume V under the membrane is large by comparison to that of the flow channel. Membrane elasticity is considered negligible. Also for dynamic calculations, variations of the state parameters are negligible inside the channel. The flow regime is laminar, stationary and the gas transformations are considered adiabatic. The mathematical model adopted after [5] and illustrated further allows determining the factors that influence the dynamic regime due to the connecting channel.

If the adiabatic exponent is k, the pressure forces that act at the extremities of a channel with a d_c diameter are:

$$F_p = \frac{\pi d_c^2}{4} p_i \,; \quad F_p^{'} = -\left(\frac{\pi d_c^2}{4}\right)^2 \frac{k p_0}{V} x_c \,. \tag{10}$$

The inertia of the gas column is:

$$F_i = \alpha \frac{\pi d_c^2}{4} l \rho \left(\frac{d^2 x_c}{dt^2}\right). \tag{11}$$

If the dynamic equilibrium equation is written for the gas column inside the channel, pressure drop due to friction, Δp_f, can be determined:

$$\Delta p_f = \lambda \frac{l}{d_c} \frac{\gamma}{2g} \left(\frac{dx_c}{dt}\right)^2 = \frac{64}{Re} \frac{\gamma l}{2 g d_c} \left(\frac{dx_c}{dt}\right)^2, \tag{12}$$

where $\lambda = 64/Re$ is the resistance coefficient. The Reynolds number can be determined by:

$$Re = \frac{d_c \rho}{\mu} \frac{dx_c}{dt}. \quad (13)$$

If *Re* is inserted in Eq. (12) the friction force equation is obtained as:

$$F_f = \frac{\pi d_c^2}{4} \Delta p_f = 8\pi\mu l \frac{dx_c}{dt}. \quad (14)$$

If it is taken into account that $x_c = 4Vp_m/\pi d_c^2 E$, the dynamic equilibrium equation for the gas column becomes:

$$p_i = p_m - 4\alpha \frac{\rho l V}{\pi d_c^2 k p_0} \frac{d^2 p_m}{dt^2} - 128 \frac{\mu l V}{\pi d_c^2 k p_0} \frac{dp_m}{dt} \quad (15)$$

It can be noticed that the equation corresponds to a second order system characterized by a characteristic pulsation ω_n and a damping ratio ζ:

$$\omega_n = \frac{d_c}{2} \sqrt{\frac{\pi k p_0}{\alpha \rho l V}}; \quad \zeta = \frac{32\mu}{d_c^2} \sqrt{\frac{Vl}{\alpha \pi k p_0 \rho}}. \quad (16)$$

For dynamic conditions, the ratio of the pressure applied to the membrane and the one at the measuring point is given by:

$$\frac{p_m}{p_i} = \frac{1}{\sqrt{\left[1 - \left(\frac{\omega}{\omega_n}\right)^2\right] + 4\zeta^2 \left(\frac{\omega}{\omega_n}\right)^2}} \quad (17)$$

The phase shift of the two values will be:

$$\varphi = arctg \left\{ \frac{\frac{-2\zeta\omega}{\omega_n}}{\left[1 - \left(\frac{\omega}{\omega_n}\right)^2\right]} \right\}. \quad (18)$$

From the last two equations it can be deduced that both pressure ratio and phase shift are variable by report to the cylinder pressure. Pressure variation due to friction during flow inside the channel is given by:

$$\Delta p_f = \lambda \frac{l}{d} \frac{\rho}{2} w^2. \quad (19)$$

Pressure variation at channel inlet is:

$$\Delta p_{ci} = \frac{\rho}{2} w^2 \left(\frac{1}{\mu_c} - 1 \right). \quad (20)$$

Pressure variation at channel outlet is:

$$\Delta p_{ce} = \frac{\rho}{2} w^2 \left[2\frac{A_c}{A_s} + \left(1 - \frac{A_c}{A_s}\right) \right]. \quad (21)$$

The gap τ between the instant when pressure varies inside the cylinder and at the transducer can be calculated by:

$$\tau = \frac{l}{w_s} \left(\frac{p_0}{p} \right)^{\frac{k-1}{2k}}. \quad (22)$$

Pressure variation corresponding to the delay τ in the transmission of the gas column inside the channel is:

$$\Delta p_\tau \approx 6n\tau p_{incr}. \quad (23)$$

The momentary pressure variation during compression is:

$$\Delta p_c = -\left(\Delta p_f + \Delta p_{ci}\right) + \Delta p_{ce} + \Delta p_\tau. \quad (24)$$

The variables entering Eqs. (19)-(24) are: λ is friction coefficient, w_s is speed of sound, n is rotation speed, μ_c is contraction coefficient.

The calculated values of pressure losses due to the connecting channel are given in Table 4.

Table 4

Pressure losses due to the connecting channel of the pressure transducer

Δp_f	Δp_{ci}	Δp_{ce}	Δp_τ	Δp_c	Δp_d
kPa					
0.4187	0.8961	0.1211	0.1081	0.1086	0.1207

5. Algorithm for the calculus of pressure in order to plot the extended diagram

Fig. 5 schematically illustrates the algorithm used for the development of a mathematical model under the Mathcad environment in order to simulate the processes that take place in an internal combustion engine. The mathematical model implies solving a distinct differential equations system for each process that takes place during a cycle of the internal combustion engine. The differential equations used in this model are mentioned in the schematic representation of the algorithm and presented explicitly further in the text. As shown by the representation in Fig. 5, the calculus is iterative and uses variable integration step. The calculus begins as soon as the intake valve closes at an angle α_{ISA} and finishes when the same valve is in its seat. Therefore, in order to determine the parameters that characterize fluids during the compression process, the following equations are employed:

– the differential equation of temperature during compression, is:

$$\frac{dT_{cil}}{d\alpha} = \frac{-\frac{dL_m}{d\alpha} - \frac{dQ_r}{d\alpha}}{\nu_{cil} C_{vcil}}; \quad (25)$$

– the equation of state for gases during compression:

$$P_{cil} = R \frac{\nu_{cil} T_{cil}}{V_{cil}} 10^4. \quad (26)$$

It was considered that the number of gas kilo moles remains constant during compression and relaxation

due to the perfect sealing ensured between piston, piston rings and cylinder.

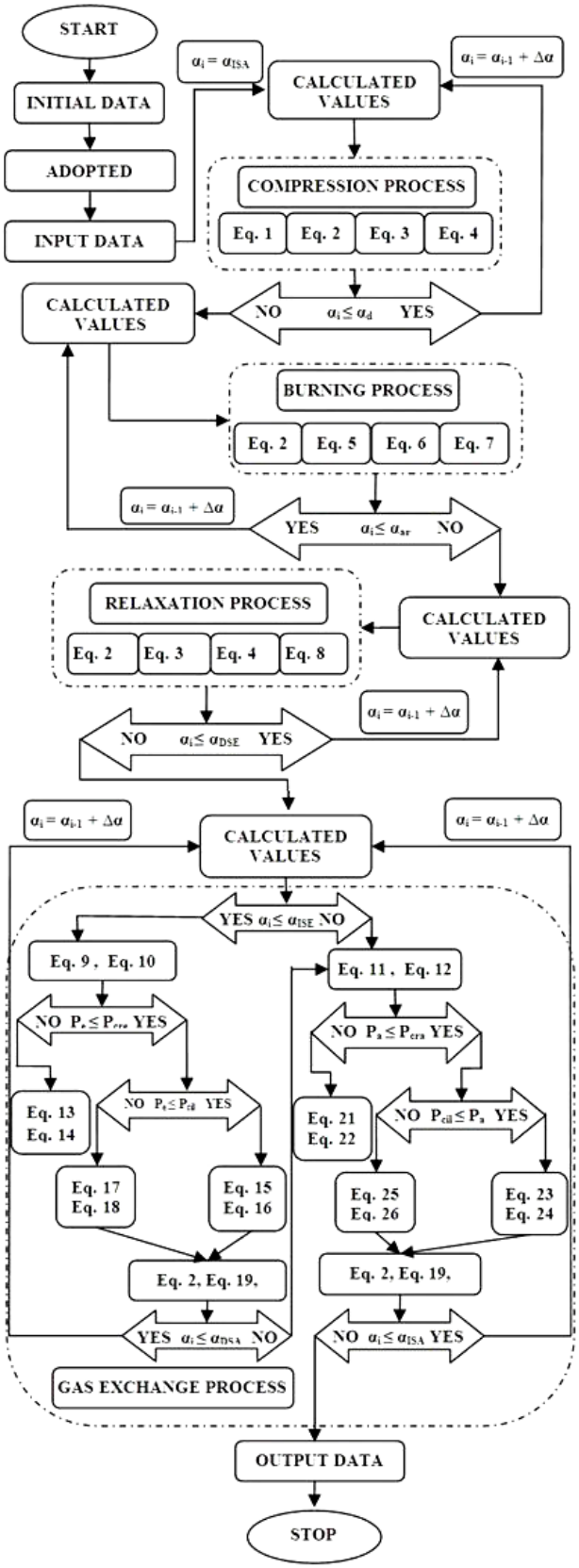

Fig. 5 Scheme of the used algorithm for simulation of processes inside an internal combustion engine

Therefore, the differential equation that describes the momentary quantity of fresh fluid inside the cylinder has the following expression:

$$\frac{d\nu}{d\alpha} = 0\,. \tag{27}$$

While the differential equation describing the momentary quantity of burnt gases present inside the cylinder is given by:

$$\frac{d\nu_{gacil}}{d\alpha} = 0\,. \tag{28}$$

Besides these equations, in order to completely evaluate the gas parameters during this process, equations such as those describing the speed of heat exchange between gasses and burning chamber walls as well as the ones describing the speed of variation for the mechanical work done are needed. The mathematical model for the burning process takes into account the following differential equations:

- the differential equation of temperature during the burning process:

$$\frac{dT_{cil}}{d\alpha} = \frac{\frac{dQ_i}{d\alpha} - \frac{dL_m}{d\alpha} - \frac{dQ_r}{d\alpha}}{\nu_{cil} C_{vcil}}\,; \tag{29}$$

- the differential equation for the momentary quantity of fresh fluid inside the cylinder:

$$\frac{d\nu_{cil}}{d\alpha} = \frac{d\xi}{d\alpha}\nu_{gpd}\left(\mu_c - 1\right); \tag{30}$$

- the differential equation for the momentary quantity of combustion gasses inside the cylinder:

$$\frac{d\nu_{gacil}}{d\alpha} = \frac{d\xi}{d\alpha}\nu_{gpd}\mu_c\,. \tag{31}$$

Also during this process, the mathematical model determines a series of parameters such as: relative speed of heat emission, absolute speed of combustion, while for the assessment of cylinder pressure the equation of state for gases is used. For the relaxation process the equations are similar to those used in the compression process. The only difference appears in the differential equation of temperature, which takes the following shape in the case of relaxation:

$$\frac{dT_{cil}}{d\alpha} = \frac{\frac{dL_m}{d\alpha} + \frac{dQ_r}{d\alpha}}{\nu_{cil} C_{vcil}}\,. \tag{32}$$

The gas exchange process is initialized at the instant of evacuation valve opening at α_{DSE} and finishes once the intake valve is back on its seat, at α_{ISA}. Over this range, the mathematical model developed for the calculus of gas exchange process parameters, uses distinct differential equations, taking into account whether the process occurs during intake or exhaust, and also according to flow regimes. At the beginning of each process during which gas exchanges take place, the manifold pressure is determined as well as the critical pressure by aid of the following equations:

$$P_e = \frac{P_0}{1 - \frac{0.601 M_{ev}\left(1+\xi_{ev}\right) W_{ge} 10^{-4}}{T_{ev}}}; \quad (33)$$

$$P_{cr.e} = P_{cil}\left(\frac{2}{k_{ev}+1}\right)^{\frac{k_{ev}}{k_{ev}-1}}; \quad (34)$$

$$P_a = \frac{P_0}{1 + \frac{0.601 M_{ev}\left(1+\xi_{ad}\right) W_{ga} 10^{-4}}{T_{ev}}}; \quad (35)$$

$$P_{cr.a} = P_a\left(\frac{2}{k_{ad}+1}\right)^{\frac{k_{ad}}{k_{ad}-1}}. \quad (36)$$

During the exhaust process, after the flow regime is established several differential equations must be solved in as appropriate to the specific situation, as follows:

- critical regime, direct flow:

$$\frac{d\nu_{cge}}{d\alpha} = \frac{2\mu s_{ev} A s_{ev} W_{cge} P_{cil}\left(\frac{2}{k_{ev}+1}\right)^{\frac{1}{k_{ev}-1}}}{n_p T_{cil}}, \quad (37)$$

$$\text{where} \quad W_{cge} = \sqrt{16640 \frac{k_{ev}}{k_{ev}+1} \frac{\mathrm{T_{cil}}}{\mathrm{M_{cil}}}}; \quad (38)$$

- sub critical regime, direct flow:

$$\frac{d\nu_{cge}}{d\alpha} = \frac{2\mu s_{ev} A s_{ev} W_{cge} P_{cil}\left(\frac{P_e}{P_{cil}}\right)^{\frac{1}{k_{ev}}}}{n_p T_{cil}}, \quad (39)$$

$$\text{where} \quad W_{cge} = \sqrt{16640 \frac{\left(1 - \frac{P_e}{P_{cil}}^{\frac{k_{ev}-1}{k_{ev}}}\right)}{\frac{k_{ev}-1}{k_{ev}}} \frac{\mathrm{T_{cil}}}{\mathrm{M_{cil}}}}; \quad (40)$$

- sub critical regime, inverse flow:

$$\frac{d\nu_{gec}}{d\alpha} = \frac{2\mu s_{ev} A s_{ev} W_{gec} P_e\left(\frac{P_{cil}}{P_e}\right)^{\frac{1}{k_{ev}}}}{n_p T_{ev}}, \quad (41)$$

$$\text{where} \quad W_{gec} = \sqrt{16640 \frac{\left(1 - \frac{P_{\mathrm{cil}}}{P_e}^{\frac{k_{ev}-1}{k_{ev}}}\right)}{\frac{k_{ev}-1}{k_{ev}}} \frac{\mathrm{T_{ev}}}{\mathrm{M_{ev}}}}. \quad (42)$$

The system of differential equations that must be solved in order to determine the cylinder work fluid parameters consists of two differential equations, to which the state equation for gasses is added. The two differential equations are:

$$\frac{dT_{cil}}{d\alpha} = \frac{1}{\nu_{cil} C_{vcil}}\left[\frac{d\nu_{gac}}{d\alpha}\left(i_{gac} - u_{cil}\right) + \frac{d\nu_{gec}}{d\alpha}\left(i_{gec} - u_{cil}\right) - \right.$$
$$\left. - \left(\frac{d\nu_{cge}}{d\alpha} + \frac{d\nu_{cga}}{d\alpha}\right)\left(i_{cil} - u_{cil}\right) - \frac{dL_m}{d\alpha} - \frac{dQ_r}{d\alpha}\right]; \quad (43)$$

$$\frac{d\nu_{cil}}{d\alpha} = \frac{d\nu_{gec}}{d\alpha} + \frac{d\nu_{gac}}{d\alpha} - \frac{d\nu_{cge}}{d\alpha} - \frac{d\nu_{cga}}{d\alpha}. \quad (44)$$

As the phenomena that take place during intake are similar to those during exhaust, after establishing the flow regime several differential equations must be solved as appropriate:

- critical regime, direct flow:

$$\frac{d\nu_{gac}}{d\alpha} = \frac{2\mu s_{ad} A s_{\mathrm{ad}} W_{gac} P_a\left(\frac{2}{k_{\mathrm{ad}}+1}\right)^{\frac{1}{k_{\mathrm{ad}}-1}}}{n_p T_{ad}}, \quad (45)$$

$$\text{where} \quad W_{gac} = \sqrt{\frac{k_{ad}-1}{k_{ad}+1} \mathrm{W_{ga}}^2 + 16640 \frac{k_{ev}}{k_{ev}+1} \frac{\mathrm{T_{ad}}}{\mathrm{M_{ad}}}}; \quad (46)$$

- sub critical regime, direct flow:

$$\frac{d\nu_{gac}}{d\alpha} = \frac{2\mu s_{\mathrm{ad}} A s_{\mathrm{ad}} W_{gac} P_a\left(\frac{P_{cil}}{P_a}\right)^{\frac{1}{k_{\mathrm{ad}}}}}{n_p T_{ad}}, \quad (47)$$

$$\text{where} \quad W_{cge} = \sqrt{16640 \frac{\left(1 - \frac{P_{cil}}{P_a}^{\frac{k_{ad}-1}{k_{ad}}}\right)}{\frac{k_{ad}-1}{k_{ad}}} \frac{\mathrm{T_{ad}}}{\mathrm{M_{ad}}}}; \quad (48)$$

- sub critical regime, inverse flow:

$$\frac{d\nu_{cga}}{d\alpha} = \frac{2\mu s_{\mathrm{ad}} A s_{\mathrm{ad}} W_{cga} P_{cil}\left(\frac{P_a}{P_{cil}}\right)^{\frac{1}{k_{\mathrm{ad}}}}}{n_p T_{cil}}, \quad (49)$$

$$\text{where} \quad W_{cga} = \sqrt{16640 \frac{\left(1 - \frac{P_{\mathrm{a}}}{P_{cil}}^{\frac{k_{ad}-1}{k_{ad}}}\right)}{\frac{k_{ad}-1}{k_{ad}}} \frac{\mathrm{T_{cil}}}{\mathrm{M_{cil}}}}. \quad (50)$$

Significance notations in Eqs. (25)-(50) is: α_i is the crankshaft angle at the current step, $\Delta\alpha$ is integration step, α_d is instant of combustion process initiation, α_{ar} is instant of combustion finish, α_{ISA} is closing angle for the intake valve, α_{DSA} is opening angle for the intake valve, α_{ISE} is closing angle for the exhaust valve, α_{DSE} is opening angle for the exhaust valve, P_a is intake manifold pressure, P_c is exhaust manifold pressure, $P_{cr,e}$ is critical pressure along exhaust route, $P_{cr.a}$ is critical pressure along intake route, P_{cil} is cylinder pressure, $dL_m/d\alpha$ is performing speed of mechanical work, $dQ/d\alpha$ is heat exchange speed, v_{cil} is kilo

moles of fluid inside the cylinder, C_{vcil} is specific heat for gases inside the cylinder, R is constant of gases, T_{cil} is gas temperature inside the cylinder, V_{cil} is momentary cylinder volume, Q_i is calorific value of the gas mixture, ξ is heat emission characteristic, v_{gpd} is kilo moles of fresh gasses at the onset of combustion, μ_c is molar expansion coefficient, M_{ev}, M_{ad} are molecular mass of the fluid inside the conduits, ξ_{ad}, ξ_{ev} are mean resistance coefficients for the intake and exhaust routes respectively, W_{ge}, W_{ga} are gas velocity inside conduits, T_{ev}, T_{ad} are gas temperatures inside conduits, k_{ev}, k_{ad} are adiabatic coefficients for the intake and exhaust processes respectively, v_{cge}, v_{cga} are number of kilo moles of fluid that pass from the cylinder to the conduits, μs_{ev}, μs_{ad} are flow coefficients for the valves, As_{ev}, As_{ad} are area of the passing cross through the valve gate, W_{gec}, W_{cge} are gas velocity through the cross-section provided by the exhaust valve, W_{cga}, W_{gac} are gas velocity through the cross-section provided by the intake valve, n_p is crankshaft rotation speed, M_{cil} is molecular mass of the working fluid, v_{gec}, v_{gac} are number of kilo moles of fluid that pass from the conduits to the cylinder, i_{gac}, i_{gec} are specific enthalpies for the fluids in the intake and exhaust conduits respectively, u_{cil} are specific internal energy of the work fluid, i_{cil} is specific enthalpy of the work fluid.

In Fig. 6 we show the results of the computations done using Mathcad for the pressure variation depending on the single-throw crankshaft rotation.

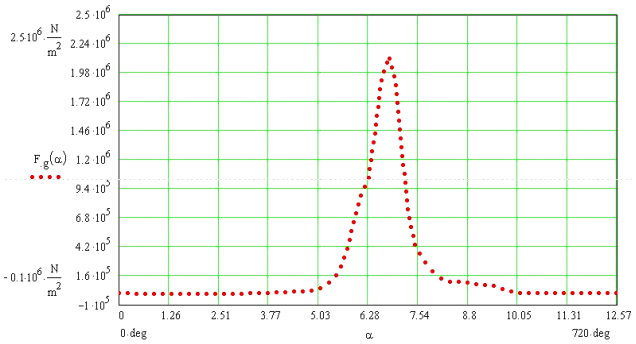

Fig. 6 Extended diagram obtained by using Mathcad computations

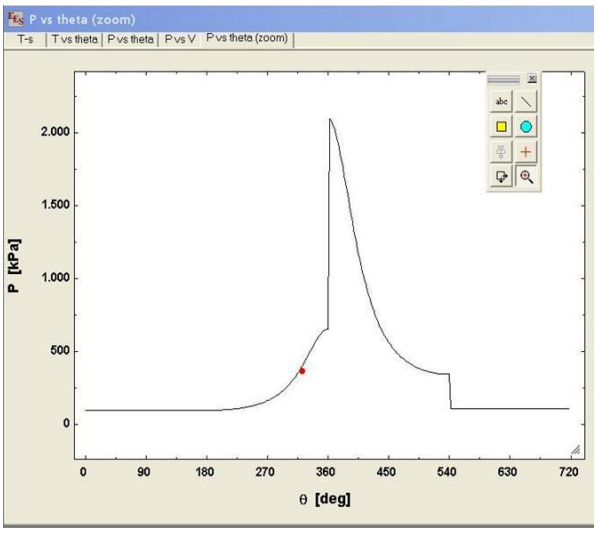

Fig. 7 Extended diagram obtained using EES 8.718D software

In order to check, by using a different method [6, 7], to see if the computed values comply with the adopted mathematical model we drew the same diagram using EES 8.718D software [8].

After entering the initial parameters and calling the calculus subroutine we obtained the extended diagram shown in Fig. 7.

It can easily be noticed that both figures show very similar shapes of the pressure curves and very close values obtained by using the two different methods.

6. Experimental results and their interpretation

The test engine is an air-cooled single-cylinder four-stroke spark ignition engine. In order to draw the experimental diagrams referenced in Fig. 8 we used an oscilloscope that has HAMEG 1507-2 memory and the SP107 software that allowed us to collect the data. Tests were performed for different regimes of the engine. The Fig. 8 shows a relevant experimental image to an extended diagram for a single cylinder four-strike cycle engine. Experience has demonstrated that a pressure transducer is suitable for accurate engine measurements.

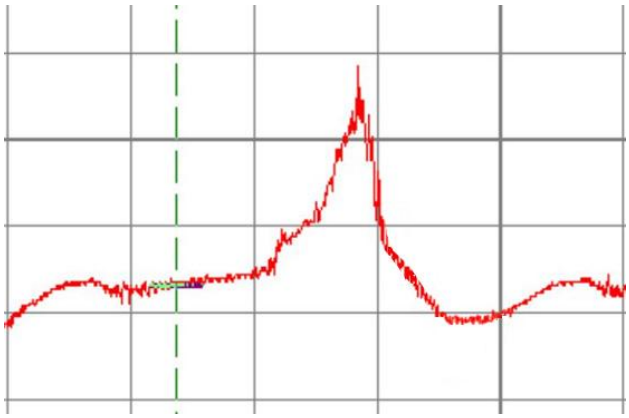

Fig. 8 Extended diagram obtained experimentally

By analyzing the extended diagram presented in Fig. 8, we can ascertain that pressure variations occur during intake, compression, burning-expansion and evacuation stage. We can clearly distinguish an area that shows strong pulsations caused by the admission valve opening. In addition, we clearly distinguish on the diagram the moment when the electric spark is generated by a pressure pin. Unfortunately, so far [1], "no technique has been standardized, however, so that the results of different investigations are not necessarily comparable – even using the same testing method".

7. Conclusions

1. A noninvasive method was advanced by modifying a spark plug so that the pressure inside the cylinder can be measured using a pressure transducer attached by a conduit. The method was found to yield results and is reliable.

2. A piezoresistive internal combustion engine transducer is developed. This transducer features a small size, capability to perform high natural frequency for fast data rates, static and dynamic measurements. This device, prove durability for the extreme engine environment.

3. In order to verify the experimental results,

comparative studies were conducted using two other methods. Starting from the described mathematical relations we created a Mathcad program with the purpose of obtaining the extended diagram for pressure and rotation angle of the single-throw crankshaft. Also, in order to verify the accuracy of the computed data we used an application of the EES software.

4. The piezoelectric transducer was calibrated for a signal of 2.000 (V/div) at 10.00 ms (Time/div) obtained with the HAMEG oscilloscope.

5. The intake valve close at 201.70° using the Mathcad model, at 202.51° using EES software and at 202.15 in the experimental situation. The corresponding average pressure was found at 0.79 kPa, for the Mathcad model, 0.82 kPa for the EES software and 0.81 kPa in the experimental situation.

6. The electrical spark is generated at 358.55° for the Mathcad model, at 361.83° for the EES software and at 359.71° for the experimental situation. The pressure obtained using the Mathcad model was of 682.42 kPa, 680.21 kPa using EES software and 681.69 kPa measured experimentally.

7. Maximum pressure was reached within the cylinder at 383.77° using the Mathcad model, at 380.62° using EES software and at 381.55° when measured experimentally. The corresponding maximum pressures were of 2070.32 kPa, for the Mathcad model, 2081.40 kPa for the EES software and 2076.45 kPa measured experimentally.

8. The exhaust valve opens at 528.33°, in the Mathcad model, at 540.00° using EES software and at 527.71° in the experimental situation. The corresponding pressures were found at 151.37 kPa, using the Mathcad model, 262.81 kPa for the EES software and 163.83 kPa measured experimentally.

9. By analyzing both the computed values and the experimental results (Figs. (6)-(8)) presented herein, we found that the obtained values are very similar for the pressure variation and time of onset process.

References

1. **Müller, H.; Winter, B.; Rohde-Brandenburger, K.** 1986. Comparative experiment with piezoelectric pressure transducers to determine their suitability for use in combustion engines, translated from MTZ Motortechnische Zeitschrift, Number 1, Franckh'sche Verlagshandlung, Stuttgard by KISTLER Instruments Ltd., 1-8.
2. **Rahmoune, M.; Osmont, D.** 2010. Classic finite elements for simulation of piezoelectric smart structures, Mechanika 6(86): 50-57.
3. **Kurtz, A.D.; Kane, A.; Goodman, S.; Landmann, W.; Geras, L.; Ned, A.A.** 2004. High Accuracy Piezoresistive Internal Combustion Engine Transducers, Kulite Semiconductor Products, Inc. Automotive Testing Expo, Messe Stuttgart, Germany, 14p.
4. **Recktenwald, G.** 2004. Pressure Transducer Calibration for M.E. Thermal Laboratory, Omega Pressure Transducer, USA, 13p.
5. **Apostolescu, N; Taraza, D.** 1979. Experimental research fundamentals of thermal machines, Bucharest, Didactic and pedagogical Publishing House: 261-273.
6. **Basshuysen, R.; Schäfer, F.** 2004. Internal Combustion Engine. Basics, Components, Systems, and Perspectives, Warrendale: SAE International, 874p.
7. **Meyer, J.** 2007. Engine modeling of an internal combustion engine with twin independent cam phasing-thesis, The Ohio State University, 92 p.
8. *****http://www.mhhe.com/engcs/mech/ees/download.html, EES –** 4 stroke engine, version 8.718D.

I. Mihai, I.C. Manolache-Rusu

BENZININIO VARIKLIO VEIKIMO DIAGRAMOS SUDARYMO METODAS

R e z i u m ė

Šis darbas susijęs su neinvazinio metodo taikymu sudarant vieno keturtakčio cilindro veikimo diagramą. Tokiai diagramai braižyti suprojektuotas eksperimentinių bandymų stendas. Pirmojoje straipsnio dalyje aprašytas pjezoelektrinis jutiklis, įgalinantis išmatuoti slėgį vidaus degimo variklio cilindre. Naudojant paminėtą programinę įrangą sudaryta vieno keturtakčio cilindro veikimo diagrama. Eksperimentiškai gautos diagramos leidžia įvertinti varomojo skysčio elgseną variklio cilindre. Tai pasiekiama analizuojant gautas kreives, palyginant proceso trukmę su skaičiavimo rezultatais, funkciniais ypatumais arba parametrų kitimo dėsniais.

I. Mihai, I.C. Manolache-Rusu

PROPOSED METHOD TO ACQUIRE AN EXTENDED DIAGRAM FOR A GASOLINE ENGINE

S u m m a r y

This paper presents a noninvasive method to obtain an extended diagram for a single cylinder four-strike cycle engine. In order to draw such a diagram we designed and built an experimental test bench. In the first part of this paper we described how one can make a piezoelectric pressure transducer that allows measuring the pressure within the internal combustion engine cylinder. We also drew the extended diagram for the single cylinder four-stroke engine using the aforementioned software. The diagrams that were obtained by means of experiment allow us to perform studies on how the motive fluid behaves inside the engine cylinder. This is achieved by studying the shape of the drawn curves, the process duration compared to the duration of the processes obtained by calculus, functionality anomalies or parameter variation laws.

Keywords: extended diagram, piezoelectric transducer, modified spark plug.

Received October 26, 2011
Accepted March 04, 2013